



# Synthesis and Characterization of Variable-Sized Silver Nanoparticles Using *Pistacia palaestina* Leaf Extract

Ishaq Musa<sup>1</sup> · Rahaf Mousa<sup>1</sup>

Received: 29 March 2024 / Accepted: 16 May 2024

© The Author(s), under exclusive licence to Springer Science+Business Media, LLC, part of Springer Nature 2024

## Abstract

*Pistacia palaestina* (*P. palaestina*) leaf extract was employed in the synthesis of spherical silver (Ag) nanoparticles, serving as a dual-purpose agent for both reduction and stabilization. These nanoparticles exhibited a range of average sizes between 2 and 27 nm. The size of these nanoparticles was observed to change in response to different concentrations of silver nitrate ( $\text{AgNO}_3$ ). This indicates that an increase in  $\text{AgNO}_3$  concentration leads to a reduction in the size of the nanoparticles. The height and morphology were analyzed using scanning probe microscopy (SPM). The crystalline nature of the Ag nanoparticles was confirmed by XRD analysis. Several properties of Ag nanoparticles, including their Raman spectroscopy, UV–visible absorption, and photoluminescence (PL), have been studied. The Raman spectroscopy revealed prominent peaks at  $585\text{ cm}^{-1}$  assigned to skeletal deformation of C–S–C and  $1580\text{ cm}^{-1}$  is linked to symmetric in plane C–C ring stretching. In the UV–visible spectrophotometry analysis, a surface plasmon resonance (SPR) band was observed, ranging between 395 and 398 nm. Additionally, the photoluminescence properties of these nanoparticles were found to vary with the excitation wavelength, marked by a distinct peak at 365 nm, a shoulder peak at 395 nm, and broader peaks observed at 470, 640, 700, and 740 nm. Furthermore, optical analyses of *P. palaestina* leaf extract indicated the presence of significant active compounds, including polyphenols, glycerol, and chlorophylls.

**Keywords** *Pistacia palaestina* · Ag nanoparticles · Raman spectroscopy · UV–visible absorbance · Photoluminescence spectroscopy

## Introduction

Nanotechnology has been a game-changer in multiple scientific arenas by allowing for the precise alteration of materials at an incredibly small scale. This has led to new capabilities and enhancements in various applications. Silver nanoparticles (AgNPs) are particularly noteworthy for their distinct features, such as superior electrical conductivity and resistance to microbial growth [1]. Their synthesis has become a focal point of research, especially given their applicability in healthcare, electronics, and eco-sciences [2–4].

Conventional techniques for creating AgNPs often require the use of toxic substances and are energy-intensive. In response to the growing focus on sustainability, researchers are investigating more environmentally friendly methods for nanoparticle production. One such innovative approach

involves leveraging plant-based extracts as reducing agents. These natural extracts contain organic compounds that can serve multiple roles in the nanoparticle formation process, including reduction and stabilization. This method not only speeds up the production process but is also cost-effective and less harmful to the environment [5, 6].

Among a variety of plants studied for this purpose, *P. palaestina*, indigenous to the Eastern Mediterranean, has shown considerable promise. Also classified scientifically as *Pistacia terebinthus*, this versatile plant can either be a tree or a shrub and is commonly found in specific Mediterranean ecosystems. It is prevalent in elevated and hilly landscapes across a range of Middle Eastern countries and nearby islands. In Arabic dialects, the fruit of this plant is often called “Butom,” and it holds various roles in local traditions [7–9].

The leaves of *P. palaestina* have a history of use in traditional medicine, offering a range of health benefits. Various techniques, from cold pressing to steam distillation, are used to extract the beneficial compounds from the leaves [10]. These natural extracts have attracted attention for their potential

✉ Ishaq Musa  
i.musa@ptuk.edu.ps

<sup>1</sup> Department of Physics, Palestine Technical University-Kadoorie, P. O. Box 7, Tulkarm, Palestine

medicinal properties, including their ability to act as antioxidants and anti-inflammatory agents [11, 12]. Chemical analysis has revealed that the plant is rich in a variety of bioactive compounds, such as flavonoids and fatty acids, which are thought to contribute to its therapeutic effects [13].

The surface-enhanced resonance of AgNPs is another aspect that makes them particularly intriguing. This phenomenon refers to the significant enhancement of electromagnetic fields around the nanoparticle surface. When AgNPs are exposed to light, the conduction electrons on the nanoparticle surface undergo collective oscillations, known as localized surface plasmon resonance (LSPR). This resonance leads to a substantial increase in the intensity of light near the particle surface, enhancing various optical properties. This unique characteristic of AgNPs has led to their widespread use in fields like sensing, imaging, and photothermal therapy. In biosensing, AgNPs enhance the detection of biomolecules, allowing for highly sensitive and specific diagnostic techniques, crucial in disease detection and management [8]. In spectroscopy, particularly in surface-enhanced Raman scattering (SERS), these nanoparticles significantly increase the Raman signals of molecules, enabling the detection of trace amounts of substances. This feature is invaluable in environmental monitoring, food safety analysis, and forensic science [14, 15].

Despite the numerous advantages, the green synthesis of silver nanoparticles and their applications in surface-enhanced resonance face challenges. Controlling the size and shape of nanoparticles during synthesis, understanding the long-term environmental impact, and ensuring scalability and reproducibility are some ongoing research areas. Future advancements in these domains are expected to address these challenges, leading to more refined and sustainable nanoparticle synthesis methods and broadening the scope of their applications in technology and medicine [16, 17].

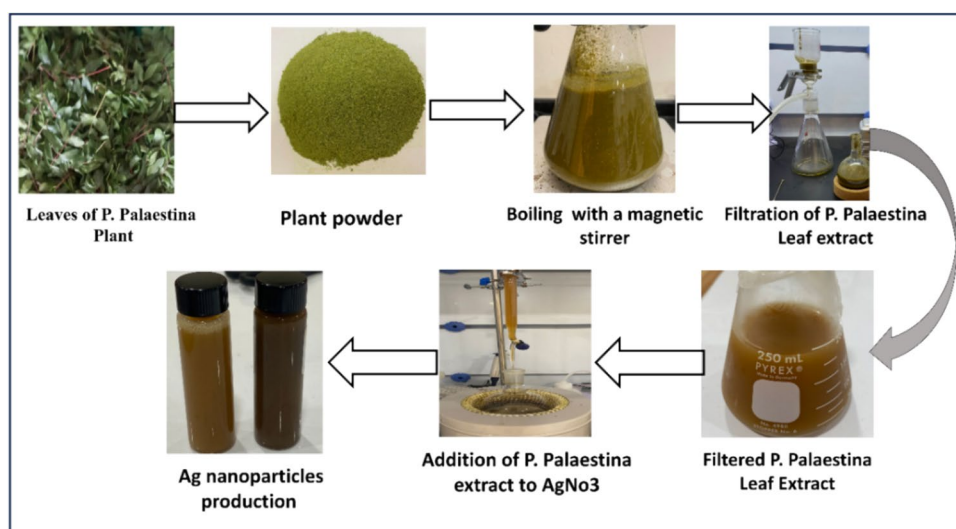
In this work, we have employed *P. palaestina* leaf extract as a novel reducing agent to fabricate Ag nanoparticles of diverse diameters. The variation in these diameters is directly influenced by the concentration of silver nitrate introduced during the synthesis process. To understand and validate the structural and optical properties of these differently sized Ag nanoparticles, we used techniques such as SPM, XRD, Raman, UV–visible absorption, and photoluminescence spectroscopy for comprehensive characterization.

## Materials and Methods

Leaves from the *P. palaestina* plant was harvested at the Al-Arroub Agricultural Station in Hebron, (West Bank, Palestine) during the summer of 2023. Silver nitrate ( $\text{AgNO}_3$ ) was used in the experiments, with distilled water serving as the solvent. Figure 1 shows the flowchart of the preparation process of leaf extract and synthesis of Ag nanoparticles. The collected samples were dried in a shaded area and subsequently ground into a fine powder using a grinding machine. Following this, 35 mg of the powdered sample was boiled in 350 mL of deionized water for half an hour. After filtration through Whatman paper and a 0.1- $\mu\text{m}$  membrane, the solution turned a light-yellow color and was stored in the refrigerator at 4 °C for further analysis and used in synthesis.

To produce silver nanoparticles of varying diameters, we prepared aqueous solutions of  $\text{AgNO}_3$  at different concentrations: 1.18 mM, 3.5 mM, 5.88 mM, and 8.24 mM, using deionized water. Subsequently, 50 mL of *P. palaestina* leaf extract was added dropwise to each 50-mL  $\text{AgNO}_3$  solution. The mixture was subsequently warmed in a heating mantle, maintaining a temperature range of 80 to 84 °C for 2 h, while being stirred continuously. The emergence of a brownish-yellow to black color signified the successful formation of

**Fig. 1** Flowchart of the preparation process of leaf extract and synthesis of Ag nanoparticles



silver nanoparticles. To separate and purify the synthesized nanoparticles, the solution was centrifuged at 10,000 rpm for 10 min. This centrifugation step was repeated five times to ensure the retrieval of pure silver nanoparticles.

The size and morphology of Ag nanoparticles were assessed using scanning probe microscopy (SPM-9700HT, Shimadzu, Japan). The measurement parameters included a scanning speed of 0.5 Hz and a resolution of

256 × 256 pixels. The spatial resolution of the device was determined to be 0.2 nm. The X-ray diffraction analysis was conducted using (Bruker D2 PHASER, Bruker, Billerica, MA, USA) with Cu  $\alpha$  radiation (30 kV and 10 mA). Raman spectroscopy was performed using a confocal Raman microscopy system Witec Alpha 300R (Ulm, Germany) with an excitation wavelength of 532 nm and laser power of 75 mW. The UV-vis absorption spectra of

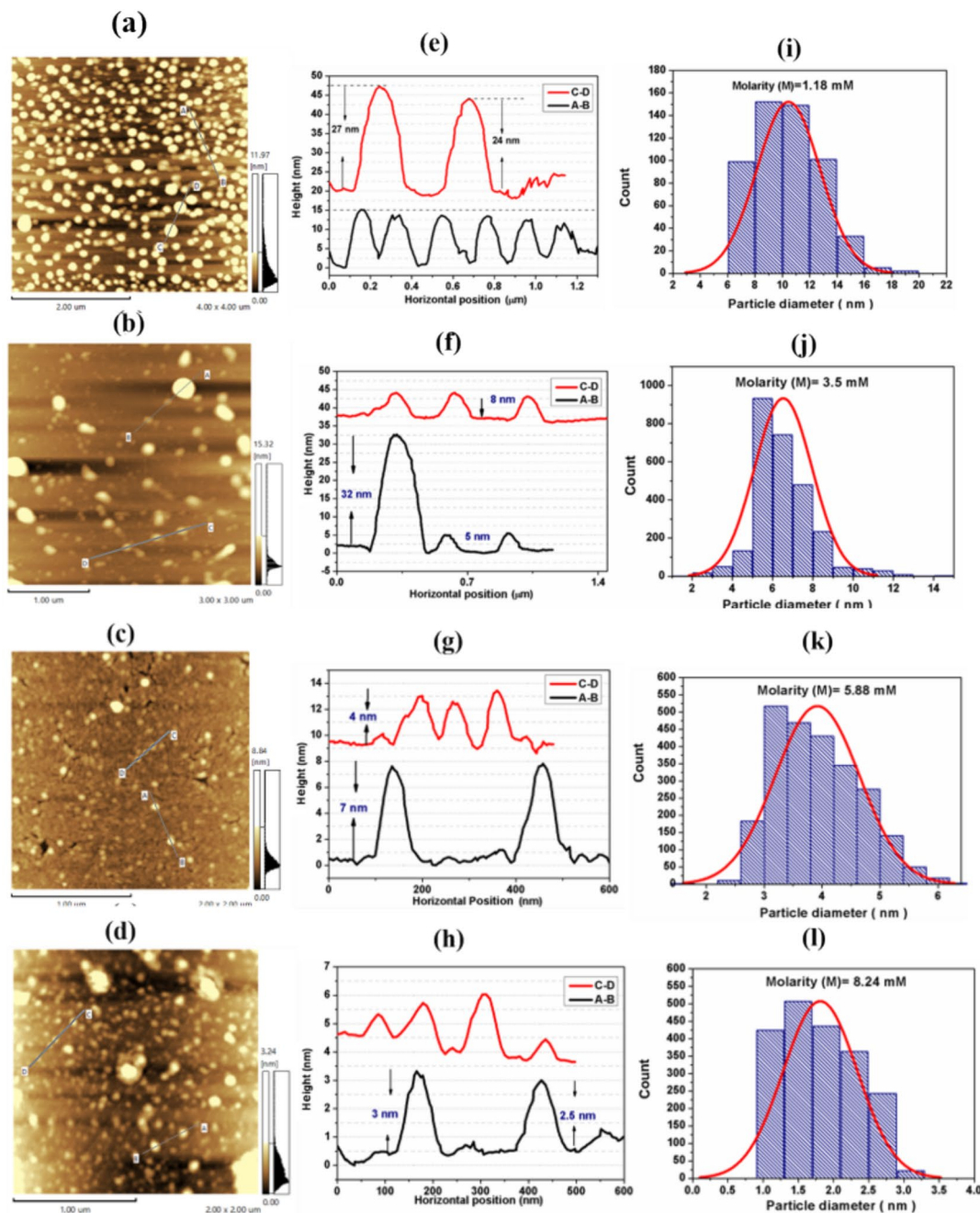


**Fig. 2** a–d Atomic force microscopy (AFM) topography images of Ag nanoparticles on a mica substrate at different concentrations (1.18, 3.5, 5.88, and 8.24 mM), scan sizes: 4 μm×4 μm, 3 μm×3 μm, 2

μm×2 μm, and 2 μm×2 μm, respectively. e–h Line profiles for nanoparticles identified in the image (a–d). i–l Particle size distribution histogram

the samples were measured on a UV-2600i (Shimadzu, Tokyo, Japan) spectrophotometer. The photoluminescence spectra were measured using RF-6000 spectrofluorometer (Shimadzu, Tokyo, Japan). The Shimadzu Lab solution software was used for data acquisition.

## Results and Discussion

### Morphology and Structure of Ag Nanoparticles

The shape and height of the Ag nanoparticles were assessed using scanning probe microscopy (SPM) topography images, captured in a non-contact dynamic mode. The AFM tip employed for this was a super sharp silicon (SSS-NCH) from Nanoworld, featuring a force constant of 42 N/m, a resonance frequency of 320 kHz, and a tip radius of 2 nm. Figure 2a–d illustrates the atomic force microscopy (AFM) topographic representation of silver nanoparticles on a mica substrate at various concentration molarities (1.18, 3.5, 5.88, and 8.24 mM). The images clearly depict the spherical morphology of the nanoparticles. Height analysis, as illustrated in Fig. 2e–g, indicates that the observed heights of these nanoparticles range from 3 to 27 nm. In Fig. 2k–n, a particle size distribution histogram for the silver nanoparticles is presented, utilizing data extracted from Fig. 2a–d that encompasses approximately 1700 nanoparticles in the image. Analysis using particle measurement software reveals that the average diameters of these nanoparticles are approximately 10 nm, 7 nm, 4 nm, and 2 nm for different concentration molarities (1.18, 3.5, 5.88, and 8.24 mM), respectively. This outcome leads to the conclusion that as the concentration of  $\text{AgNO}_3$  increases, the size of Ag nanoparticles decreases. This trend is clearly depicted in Fig. 3 where the concentration of silver nitrate ( $\text{AgNO}_3$ )

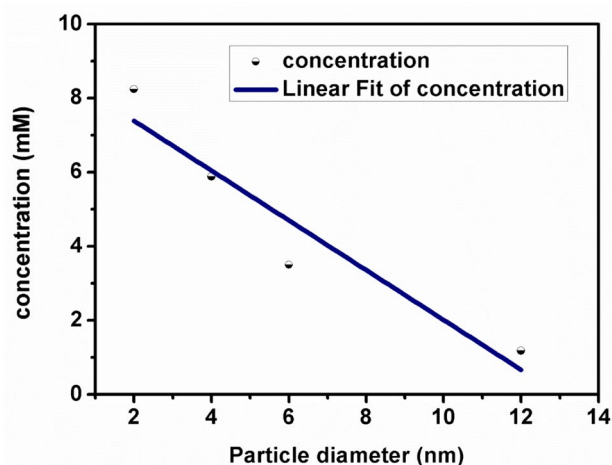


**Fig. 3** The influence of  $\text{AgNO}_3$  concentration on the diameter of Ag nanoparticles

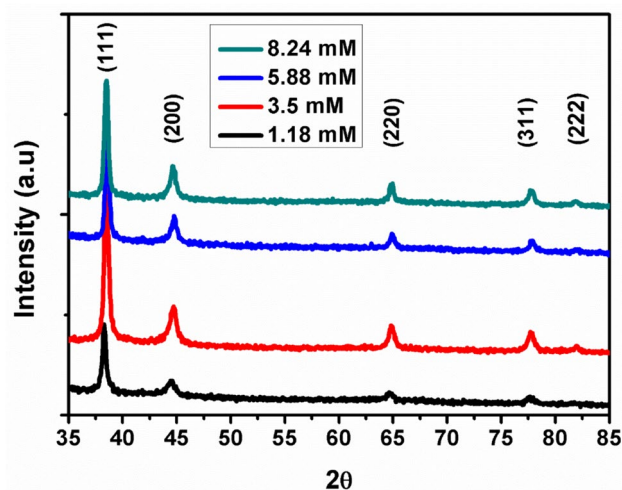


**Fig. 4** X-ray diffraction pattern of the silver nanoparticles for different concentration molarities (1.18, 3.5, 5.88, and 8.24 mM) deposited on a glass substrate

significantly influences the characteristics of the produced silver nanoparticles. The pattern observed can be interpreted using the principles of nucleation and growth. Higher  $\text{AgNO}_3$  concentrations accelerate the nucleation process, leading to the formation of many tiny clusters. These clusters serve as the foundational units for the nanoparticles. This dynamic interaction between the precursor concentration and the nucleation process accounts for the decrease in nanoparticle size as the  $\text{AgNO}_3$  concentration increases [2, 18].

Figure 4 displays the X-ray diffraction (XRD) patterns for the Ag nanoparticles for different concentration molarities (1.18, 3.5, 5.88, and 8.24 mM), verifying their face-centered cubic lattice structure. All the Ag nanoparticles display consistent diffraction profiles, featuring distinct peaks at  $2\theta$  angles of  $38.5^\circ$ ,  $44.5^\circ$ ,  $65.0^\circ$ ,  $77.5^\circ$ , and  $82.0^\circ$ . These peaks correspond to the (111), (200), (220), (311), and (222) crystallographic planes of face-centered cubic crystals, respectively. The data obtained is in well agreement with the literature report of JCPDS-File No. 04-0783 [19, 20].

### Raman Spectroscopy of Ag Nanoparticles

Surface enhanced Raman spectroscopy (SERS) is a well-known and extensively researched technique for characterizing metal nanoparticles. To determine the possible functional groups of capping agents involved in the stability of silver nanoparticles [21], Raman spectrum of the Ag nanoparticles was recorded as shown in Fig. 5. It consists of vibrational modes at 248, 360, 482, 585, 652, 1098, 1347, and  $1580\text{ cm}^{-1}$ . The *P. palaestina* leaf extract contained several organic constituents such as carboxylic and hydroxyl groups. In Raman spectra, the peak at  $248\text{ cm}^{-1}$ , which is identified and attributed specifically to the stretching

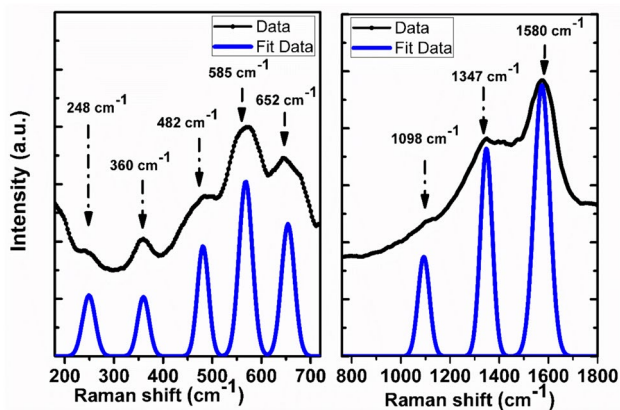


**Fig. 5** Raman spectrum and deconvolution results of silver nanoparticles deposited on glass substrate

vibrations found in the silver-nitrogen (Ag–N) bond [22]. The vibrational mode observed at the peak position of  $360\text{ cm}^{-1}$  is attributed to the in-plane bending of the C–C–Cl bond [23]. The skeletal deformation of C–N–C is observed around  $482\text{ cm}^{-1}$  [24]. The features at  $585\text{ cm}^{-1}$  assigned to skeletal deformation of C–S–C. The other band at  $652\text{ cm}^{-1}$  was related to stretching S–C. The peak  $1098\text{ cm}^{-1}$  belongs to in-plane C–C–H bend and C–C–S bend [25]. The peak at  $1347\text{ cm}^{-1}$  is linked to bending (CH<sub>2</sub>) and bending (C–O–H) and the symmetric in plane C–C ring stretching is observed at around  $1580\text{ cm}^{-1}$  [26, 27]. Thus, from the preferential enhancement of these Raman bands, it can be concluded that the carboxylate groups of the *P. palaestina* are involved in the capping of the silver nanoparticles [21].

### Absorption and Photoluminescent of *P. palaestina* Leaf Extract

Figure 6 illustrates the absorption characteristics of *P. palaestina* leaf extract, as measured by a UV–vis spectrophotometer. The absorption spectrum of *P. palaestina* is distinguished by prominent bands with several peaks occurring at wavelengths of 225, 267, 355, and 670 nm. The initial two peaks, at 225 nm and 267 nm, are likely due to the presence of phenolic compounds such as quinic acid, gallic acid, trigalloylglucose acid, and tetragalloylquinic acid in the leaf extract [13]. These compounds are known to serve as coating agents and play a crucial role in the reduction process during the synthesis of silver nanoparticles. The absorption peak observed at 355 nm is linked to glycerol, which plays a crucial role as a stabilizer in the synthesis of silver nanoparticles [28, 29]. Additionally, the inset of Fig. 6 highlights an absorption peak at 670 nm, suggesting the presence of chlorophyll [30, 31].

The photoluminescence spectra of *P. palaestina*, depicted in Fig. 7, were observed at various excitation wavelengths, revealing distinctive features that can be attributed to specific

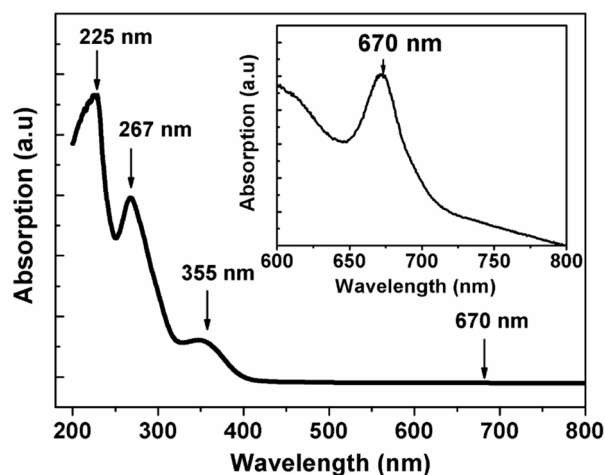


**Fig. 6** UV–Vis spectrum of the aqueous extract leaves of the *P. palaestina* at wavelength 200 to 800 nm

compounds present in the sample. The spectrum suggests that tocopherols and phenols are responsible for the shorter wavelength band observed in the total fluorescence spectra. Upon exciting the solution extract from *P. palaestina* with a 200-nm wavelength, two prominent emission peaks are observed. The first peak, located at 248 nm, is associated with phenol compounds. The second peak, found at a position of 365 nm, corresponds to the presence of glycerol in the extract. Furthermore, when the extract is excited at a wavelength of 270 nm, both the phenolic and glycerol compounds exhibit a broad and red-shifted emission peak at 325 nm, along with a distinct shoulder at 395 nm [32], as depicted in Fig. 7b. The fluorescence analysis of *P. palaestina* leaf extract leverages the presence of naturally occurring fluorescent components, including phenolic compounds, tocopherols, pheophytins, and their oxidation products. These compounds demonstrate comparable UV-absorption and fluorescence characteristics, as indicated [33].

Figure 7c displays a prominent long-wavelength band in the spectra of *P. palaestina*. When excited at a wavelength of 420 nm, this band exhibits emission in the range of 600 to 750 nm. Within this spectrum, two distinct peaks are apparent: a pronounced peak at 680 nm and a broader peak around 730 nm. These peaks are indicative of the presence of chlorophyll and pheophytin, respectively. These findings align with the research reported by Musa [31], which details the distinct spectral properties typical of these compounds. The leaf extract of *P. palaestina* displays intense luminescence, attributed to the presence of chlorophyll. To investigate this, a UV lamp with a wavelength of 365 nm and a power of 15 W was employed. As depicted in Fig. 7d, under UV light, the leaf extract of *P. palaestina* exhibits a distinct pink and orange luminosity.

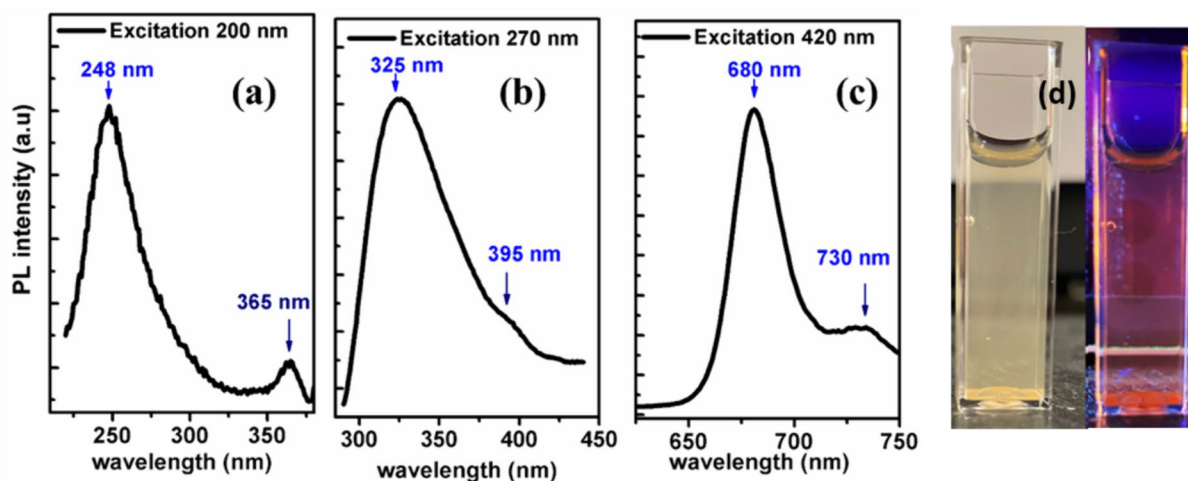


**Fig. 7** Emission spectrum of *P. Palaestina* leaf extract with **a**  $\lambda_{ex}=200$  nm. **b**  $\lambda_{ex}=270$  nm. **c**  $\lambda_{ex}=420$  nm. **d** *P. palaestina* leaf extract under UV light

### Absorption and Photoluminescent of Ag Nanoparticles

Silver nanoparticles (AgNPs) exhibit exceptional optical properties, including absorption and photoluminescence, which are influenced by their size, shape, and surrounding medium. The hallmark of these properties is surface plasmon resonance (SPR), which results in a strong absorption band in the visible spectrum, giving AgNPs distinct colors. AgNPs can also exhibit photoluminescence by absorbing and re-emitting light at longer wavelengths, although this effect is typically more subtle compared to other materials [34]. Figure 8 illustrates the UV–visible absorption spectra of silver nanoparticles (AgNPs) at different silver ion concentrations: 1.18, 3.5, 5.88, and 8.24 mM. Silver features free electrons on its surface, and the observed surface plasmon resonance (SPR) absorption band is formed by the synchronous resonance of these electrons with the

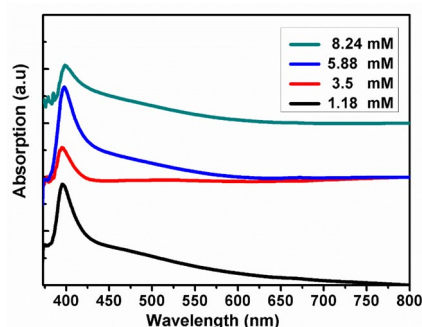


**Fig. 8** UV–visible absorption spectra of silver nanoparticles for different concentration molarities (1.18, 3.5, 5.88, and 8.24 mM)

electromagnetic wave of the incoming light. This UV–vis spectroscopy analysis is crucial for monitoring the reduction process from  $Ag^+$  to  $Ag^0$ . The appearance of peaks in the spectra signifies the SPR characteristics of AgNPs [35].

Each sample's spectrum predominantly shows a single absorption peak. The SPR bands were found within the 395 to 398 nm range, consistent with typical properties of silver nanoparticles. Variations in the SPR band, attributed to aggregated and different-sized nanoparticles, were observed, as highlighted by Bamsaoud et al. [36].

Furthermore, the position of the SPR band in UV–Vis spectra is affected by several factors: particle size, shape, dynamics of charge transfer between the nanoparticles and the medium, their interaction with the medium, and the local refractive index [37]. Photoluminescence serves as a key technique in determining the optical characteristics of silver nanoparticles as photonic materials. Investigations included recording fluorescence emission at various concentrations under two excitation wavelengths: 210 nm and 250 nm as shown in Fig. 9a, b. This analysis revealed multiple emission peaks in fluorescence, spanning a range of 300 to 800 nm. Notably, each excitation wavelength produced distinct, intense peaks which were consistent across all concentrations tested. The fluorescence of these nanoparticles varied with the excitation wavelength. A notable observation was a sharp peak at 365 nm, a shoulder peak at 395 nm, and broader peaks at 470, 640, 700, and 740 nm. Peaks at 365 and 470 nm were aligned with surface plasmon resonance seen in UV–visible spectroscopy, suggesting that fluorescence mainly arises from single-electron transitions between specific energy states [38]. Excitation at the shorter wavelength of 210 nm resulted in a pronounced emission peak at 365 nm, alongside weaker

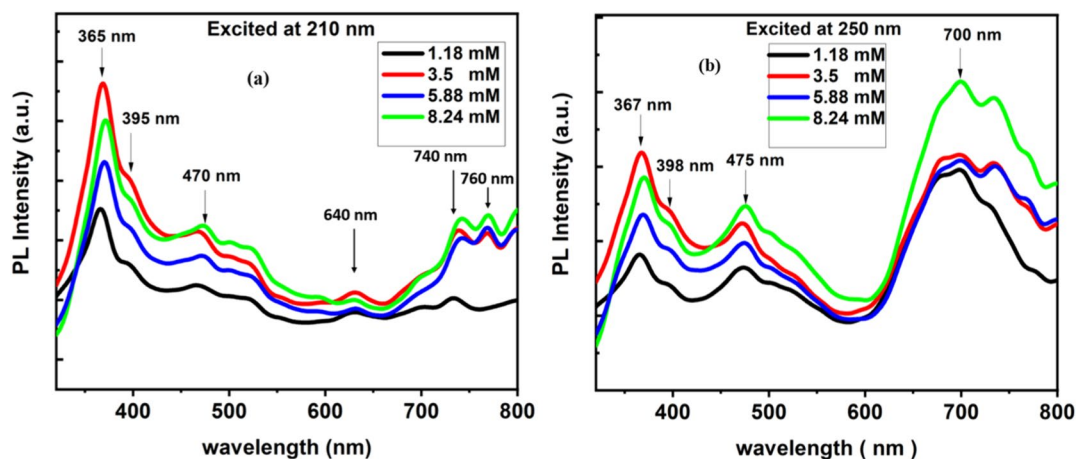


**Fig. 9** Photoluminescence spectra of silver nanoparticles of various concentrations AgNO<sub>3</sub> at different excitation wavelengths: **a** 210 nm and **b** 250 nm

and broader peaks at 395, 470, 640, and 740 nm. Conversely, excitation at the longer wavelength of 250 nm reduced the intensity of the 365 nm peak while enhancing and broadening other resonance peaks at 475 and 700 nm. This variance in excitation and emission is attributed to the presence of both small and large nanoparticles, as well as aggregated nanoparticles [39, 40]. As the excitation wavelength increases, the emission peak's intensity diminishes, and the 365-nm peak experiences a slight red shift. The red shift observed in the fluorescence spectrum occurs because electrons are energized to energy levels that are lower when exposed to longer excitation wavelengths. Consequently, their relaxation also happens at these extended wavelengths [41]. Furthermore, as the excitation wavelength lengthens, it may deviate from the nanoparticles' optimal resonance conditions. This deviation can result in a diminished light absorption efficiency, which in turn causes a decrease in the intensity of the emission. Additionally, quantum confinement in nanoparticles plays a significant role, especially as the particle size nears the exciton Bohr radius. In such quantum confined states, the electronic properties of the nanoparticles differ from those in bulk materials, influencing the absorption and emission spectra. The interaction between the increased excitation wavelength and this quantum-confined states can cause alterations in the emission spectrum, manifesting as shifts in its characteristics [42, 43].

## Conclusion

This research successfully establishes a cost-effective, environmentally friendly method for synthesizing AgNPs using native *P. palaestina* leaf extract, offering a

sustainable alternative to conventional chemical methods. The resultant nanoparticles were spherical and varied in size from 2 to 27 nm, with a notable correlation between the concentration of silver nitrate (AgNO<sub>3</sub>) and nanoparticle size—higher AgNO<sub>3</sub> concentrations resulted in smaller nanoparticles. Scanning probe microscopy (SPM) effectively analyzed their height and morphology, while X-ray diffraction (XRD) analysis confirmed their crystalline nature. The study's investigation into various properties of the Ag nanoparticles, using techniques like Raman spectroscopy, UV-visible absorption, and photoluminescence (PL), yielded significant findings. Raman spectroscopy identified prominent peaks at 585 cm<sup>-1</sup> and 1580 cm<sup>-1</sup>, indicating specific molecular vibrations. The UV-visible spectrophotometry analysis observed a surface plasmon resonance (SPR) band between 395 and 398 nm, which is characteristic of Ag nanoparticles. The photoluminescence properties varied with the excitation wavelength, showing distinct peaks at 365 nm, a shoulder peak at 395 nm, and broader peaks at 470 and 690 nm. These variations in photoluminescence are indicative of the diverse electronic environments within the nanoparticles. Additionally, the optical analyses of the *P. palaestina* leaf extract revealed the presence of significant bioactive compounds such as polyphenols, glycerol, and chlorophylls. These compounds likely contribute to the effective reduction and stabilization of the Ag nanoparticles. This study not only advances the understanding of green synthesis of nanoparticles but also highlights the potential of using natural extracts in nanotechnology, opening avenues for environmentally friendly and sustainable synthesis methods. The ability to tune these optical properties by altering the size, shape, and dielectric environment of the nanoparticles adds to their versatility and appeal in scientific and industrial

applications. Therefore, future research could explore further optimization of synthesis parameters to fine-tune nanoparticle properties for specific applications, as well as investigate the broader implications of using green synthesis methods in various fields.

**Acknowledgements** The authors thank Palestine Technical University-Kadoorie (PTUK) for the facilities and support. We also thanks Prof. Hassan Arafat from Khalifa University for his collaboration.

**Author Contributions** Ishaq Musa: writing—review and editing, writing—original draft, visualization, methodology, investigation, conceptualization, and formal analysis; Rahaf Mousa: writing—review and editing, investigation, and data curation.

**Data Availability** All data in this study are available from the corresponding author upon request.

## Declarations

**Competing Interests** The authors declare no competing interests.

## References

- Ahmed MD, Maraz KM, Shahida S et al (2021) A review on the synthesis, surface modification and drug delivery of nanoparticles. *GJETA* 8:032–045. <https://doi.org/10.30574/gjeta.2021.8.2.0114>
- Kaabipour S, Hemmati S (2021) A review on the green and sustainable synthesis of silver nanoparticles and one-dimensional silver nanostructures. *Beilstein J Nanotechnol* 12:102–136. <https://doi.org/10.3762/bjnano.12.9>
- Amen R, Mukhtar A, Saqib S et al (2021) Chapter 1 - history and development of nanomaterials. In: Tahir MB, Sagir M, Asiri AM (eds) *Nanomaterials: synthesis, characterization, hazards and safety*. Elsevier, pp 1–14
- Singh J, Dutta T, Kim K-H et al (2018) ‘Green’ synthesis of metals and their oxide nanoparticles: applications for environmental remediation. *Journal of Nanobiotechnology* 16:84. <https://doi.org/10.1186/s12951-018-0408-4>
- Prakash M, Kavitha HP, Abinaya S, Vennila JP, Lohita D (2022) Green synthesis of bismuth based nanoparticles and its applications - a review. *Sustain Chem Pharm* 25:100547. <https://doi.org/10.1016/J.SCP.2021.100547>
- Kshetriya V, Koshti B, Gour N (2021) Chapter four - green synthesized nanoparticles: classification, synthesis, characterization, and applications. In: Verma SK, Das AK (eds) *Comprehensive Analytical Chemistry*. Elsevier, pp 173–222
- Al-Marazeeq KM, Al-Ismail K, Saleh M (2022) Butom (*Pistacia palaestina*, Boiss) fruit and its extracted oil functional characteristics. *Rivista Italiana Delle Sostanze Grasse*. [https://www.innovhub-ssi.it/kdocs/2048252/2022\\_vol\\_991\\_-\\_art\\_03\\_-\\_al-marazeeq.pdf](https://www.innovhub-ssi.it/kdocs/2048252/2022_vol_991_-_art_03_-_al-marazeeq.pdf)
- Flamini G, Bader A, Cioni PL et al (2004) Composition of the essential oil of leaves, galls, and ripe and unripe fruits of Jordanian *Pistacia palaestina* Boiss. *J Agric Food Chem* 52:572–576. <https://doi.org/10.1021/jf034773t>
- Davidovich-Rikanati R, Bar E, Hivert G et al (2022) Transcriptional up-regulation of host-specific terpene metabolism in aphid-induced galls of *Pistacia palaestina*. *J Exp Bot* 73:555–570. <https://doi.org/10.1093/jxb/erab289>
- Zhang Q-W, Lin L-G, Ye W-C (2018) Techniques for extraction and isolation of natural products: a comprehensive review. *Chin Med* 13:20. <https://doi.org/10.1186/s13020-018-0177-x>
- Grover M (2021) *Pistacia integerrima* (Shringi)- A plant with significant pharmacological activities. *J Phytopharmacol* 10:323–330. <https://doi.org/10.31254/phyto.2021.10508>
- Pharmacological investigation of genus *Pistacia* | IntechOpen. <https://www.intechopen.com/chapters/76486>. Accessed 12 Sep 2023
- Ben Ahmed Z, Yousfi M, Viaene J et al (2021) Four *Pistacia atlantica* subspecies (*atlantica*, *cabulica*, *kurdica* and *mutica*): a review of their botany, ethnobotany, phytochemistry and pharmacology. *J Ethnopharmacol* 265:113329. <https://doi.org/10.1016/j.jep.2020.113329>
- Ondieki AM, Birech Z, Kaduki KA et al (2023) Fabrication of surface-enhanced Raman spectroscopy substrates using silver nanoparticles produced by laser ablation in liquids. *Spectrochim Acta Part A Mol Biomol Spectrosc* 296:122694. <https://doi.org/10.1016/j.saa.2023.122694>
- Chang Y-L, Su C-J, Lu L-C, Wan D (2022) Aluminum plasmonic nanoclusters for paper-based surface-enhanced Raman spectroscopy. *Anal Chem* 94:16319–16327. <https://doi.org/10.1021/acs.analchem.2c03014>
- Madhu SR, Bharti R (2023) A review on the synthesis and photocatalytic application of silver nano particles. *IOP Conf Ser: Earth Environ Sci* 1110:012021. <https://doi.org/10.1088/1755-1315/1110/1/012021>
- Devadharshini R, Karpagam G, Pavithra K et al (2023) Green synthesis of silver nanoparticles *MRJI* 33:1–9. <https://doi.org/10.9734/mrji/2023/v33i51380>
- Osorio-Echavarría J, Osorio-Echavarría J, Ossa-Orozco CP, Gómez-Vanegas NA (2021) Synthesis of silver nanoparticles using white-rot fungus *anamorphous Bjerkandera* sp. R1: influence of silver nitrate concentration and fungus growth time. *Sci Rep* 11:3842. <https://doi.org/10.1038/s41598-021-82514-8>
- Singh H, Du J, Singh P, Yi TH (2018) Extracellular synthesis of silver nanoparticles by *Pseudomonas* sp. THG-LS1.4 and their antimicrobial application. *Journal of Pharmaceutical Analysis* 8:258–264. <https://doi.org/10.1016/j.jpha.2018.04.004>
- Ghasemi S, Dabirian S, Kariminejad F et al (2024) Process optimization for green synthesis of silver nanoparticles using *Rubus discolor* leaves extract and its biological activities against multi-drug resistant bacteria and cancer cells. *Sci Rep* 14:4130. <https://doi.org/10.1038/s41598-024-54702-9>
- Joshi N, Jain N, Pathak A et al (2018) Biosynthesis of silver nanoparticles using *Carissa carandas* berries and its potential antibacterial activities. *J Sol-Gel Sci Technol* 86:682–689. <https://doi.org/10.1007/s10971-018-4666-2>
- Xiao G-N, Man S-Q (2007) Surface-enhanced Raman scattering of methylene blue adsorbed on cap-shaped silver nanoparticles. *Chem Phys Lett* 447:305–309. <https://doi.org/10.1016/j.cplett.2007.09.045>
- Izquierdo-Lorenzo I, Sanchez-Cortes S, Garcia-Ramos JV (2010) Adsorption of beta-adrenergic agonists used in sport doping on metal nanoparticles: a detection study based on surface-enhanced Raman scattering. *Langmuir* 26:14663–14670. <https://doi.org/10.1021/la102590f>
- Zannotti M, Rossi A, Giovannetti R (2020) SERS activity of silver nanosphere, triangular nanoplates, hexagonal nanoplates and quasi-spherical nanoparticles: effect of shape and morphology. *Coatings* 10:288. <https://doi.org/10.3390/coatings10030288>
- Madzharova F, Heiner Z, Kneipp J (2020) Surface-enhanced hyper Raman spectra of aromatic thiols on gold and silver nanoparticles. *J Phys Chem C* 124:6233–6241. <https://doi.org/10.1021/acs.jpcc.0c00294>
- Jeon GW, Lee S-H, Jang J-W (2022) Opposite Raman shift of ring stretching dependent on the coordinated silver volume in



- surface-enhanced Raman spectroscopy of polypyrrole. *J Phys Chem Lett* 13:1300–1306. <https://doi.org/10.1021/acs.jpcclett.1c04069>
27. Hernández-Arteaga AC, Delgado-Nieblas FC, Ojeda-Galván HJ et al (2017) Surface-enhanced Raman spectroscopy of acetylneuraminic acid on silver nanoparticles: role of the passivating agent on the adsorption efficiency and amplification of the Raman signal. *J Phys Chem C* 121:21045–21056. <https://doi.org/10.1021/acs.jpcc.7b07186>
  28. Aires A, Marrinhas E, Carvalho R et al (2016) Phytochemical composition and antibacterial activity of hydroalcoholic extracts of *Pterospartum tridentatum* and *Mentha pulegium* against *Staphylococcus aureus* isolates. *Biomed Res Int* 2016:1–11. <https://doi.org/10.1155/2016/5201879>
  29. Murillo-Acevedo YS, Giraldo L, Poon PS et al (2021) The Cramer's rule for the parametrization of phenol and its hydroxylated byproducts: UV spectroscopy vs. high performance liquid chromatography. *Environ Sci Pollut Res* 28:6746–6757. <https://doi.org/10.1007/s11356-020-10897-8>
  30. Nogay G, Hilal A, Gunduz L et al (2019) Determination of the chlorophyll content of pistachio (*Pistacia vera* L.) kernels using various extraction techniques. *J Proc Ener Agri* 23:199–201. <https://doi.org/10.5937/JPEA1904199N>
  31. Musa I (2024) Investigation the optical properties of Palestinian olive oils for different geographical regions by optical spectroscopy technique. *Food Chemistry Advances* 4:100584. <https://doi.org/10.1016/j.focha.2023.100584>
  32. Dodiuk H, Kosower EM (1975) Multiple fluorescences from the excited state of N-methyl-2-N-phenyl-amino-6-naphthalenesulphonate in glycerol: Fast proton transfer. *Chem Phys Lett* 34:253–257. [https://doi.org/10.1016/0009-2614\(75\)85266-3](https://doi.org/10.1016/0009-2614(75)85266-3)
  33. Barbieri D, Gabriele M, Summa M et al (2020) Antioxidant, nutraceutical properties, and fluorescence spectral profiles of bee pollen samples from different botanical origins. *Antioxidants* 9:1001. <https://doi.org/10.3390/antiox9101001>
  34. Gangwar MS, Agarwal P (2023) Plasmon-enhanced photoluminescence and Raman spectroscopy of silver nanoparticles grown by solid state dewetting. *J Phys Condens Matter*. <https://doi.org/10.1088/1361-648X/acd1cd>
  35. Anandalakshmi K, Venugobal J, Ramasamy V (2016) Characterization of silver nanoparticles by green synthesis method using *Pedaliumpurex* leaf extract and their antibacterial activity. *Appl Nanosci* 6:399–408. <https://doi.org/10.1007/s13204-015-0449-z>
  36. Bamsaoud SF, Basuliman MM, Bin-Hameed EA et al (2021) The effect of volume and concentration of AgNO<sub>3</sub> aqueous solutions on silver nanoparticles synthesized using *Ziziphus Spina-Christi* leaf extract and their antibacterial activity. *J Phys: Conf Ser* 1900:012005. <https://doi.org/10.1088/1742-6596/1900/1/012005>
  37. Xin X, Qi C, Xu L et al (2022) Green synthesis of silver nanoparticles and their antibacterial effects. *Front Chem Eng* 4:941240. <https://doi.org/10.3389/fceng.2022.941240>
  38. Zhao Y, Lim M, Choi S, Yu J (2022) Excitation spectrum, nanoparticles, and their applications in cellular optical imaging. *J Biol Educ* 56:122–129. <https://doi.org/10.1080/00219266.2020.1757483>
  39. Musa I, Qamhieh N, Mahmoud ST (2023) Ag nanocluster production through DC magnetron sputtering and inert gas condensation: a study of structural, Kelvin probe force microscopy, and optical properties. *Nanomaterials* 13:2758. <https://doi.org/10.3390/nano13202758>
  40. Tafur G, Benndorf C, Acosta D et al (2019) Optical properties of silver nanoparticles embedded in dielectric films produced by dc and rf magnetron sputtering. *J Phys: Conf Ser* 1173:012004. <https://doi.org/10.1088/1742-6596/1173/1/012004>
  41. Parang Z, Keshavarz A, Farahi S et al (2012) Fluorescence emission spectra of silver and silver/cobalt nanoparticles. *Scientia Iranica* 19:943–947. <https://doi.org/10.1016/j.scient.2012.02.026>
  42. Yao Y, Biswas S, Kang M et al (2022) Explanation of the opposing shifts in the absorption edge and the optical resonance in CuFeS<sub>2</sub> nanoparticles. *J Phys Chem C* 126:5592–5597. <https://doi.org/10.1021/acs.jpcc.1c07956>
  43. Garoufalis CS, Zeng Z, Bester G et al (2022) Excitons in ZnO quantum dots: the role of dielectric confinement. *J Phys Chem C* 126:2833–2838. <https://doi.org/10.1021/acs.jpcc.1c09702>

**Publisher's Note** Springer Nature remains neutral with regard to jurisdictional claims in published maps and institutional affiliations.

Springer Nature or its licensor (e.g. a society or other partner) holds exclusive rights to this article under a publishing agreement with the author(s) or other rightsholder(s); author self-archiving of the accepted manuscript version of this article is solely governed by the terms of such publishing agreement and applicable law.